Thermodynamic Control of Halogen-Terminated Silicon Nanoparticle Morphology

ARTICLE *in* CRYSTAL GROWTH & DESIGN · SEPTEMBER 2014

Impact Factor: 4.89 · DOI: 10.1021/cg500558j

2 AUTHORS, INCLUDING:

Amanda S Barnard
The Commonwealth Scientific and Industrial …

181 PUBLICATIONS **4,318** CITATIONS

SEE PROFILE

CRYSTAL GROWTH & DESIGN

Article

pubs.acs.org/crystal

Thermodynamic Control of Halogen-Terminated Silicon Nanoparticle Morphology

Hugh F. Wilson* and Amanda S. Barnard

CSIRO Materials Science & Engineering, 343 Royal Pde, Parkville, Victoria 3052, Australia

Supporting Information

ABSTRACT: The fabrication of silicon nanoparticles terminated with halogen species provides a convenient route to create readily functionalizable nanostructures; however, the relationship between formation conditions and the thermodynamic ground-state morphology of the nanoparticles thus formed remains poorly understood. In this work, we use density functional theory calculations to compute surface energies of silicon surfaces terminated with fluorine, chlorine, bromine, and iodine as a function of halogen chemical potential and hence we compute, via a nanomorphology model, the thermodynamically optimal morphology of halogen-terminated silicon nanoparticles. We predict a variety of optimal nanoparticle shapes consisting primarily of Si(100), Si(113), and Si(111) facets with varying terminations, and we demonstrate how control over morphology may be attained by controlling the chemical environment. Implications for the fabrication of nanoparticles with facet-selective reactivity are also discussed.

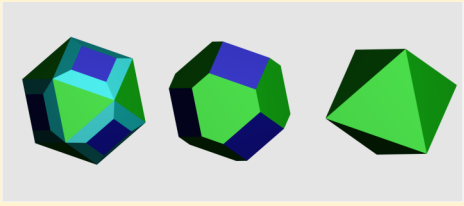

INTRODUCTION

Silicon nanoparticles and quantum dots present a broad range of technological applications in areas such as energy storage,[1,2] photovoltaics,[3] nanomedicine,[4] and optoelectronics.[5] The formation of silicon nanoparticles may be achieved by a wide variety of methods in the solid, liquid, gas, or plasma phase,[5] variously producing freestanding or solid-embedded nanoparticles, with a variety of possible terminating species on the surface. Depending on the fabrication method and formation conditions, nanoparticle shape may be dependent either on the kinetics of the process or on the thermodynamically optimal shape, and various methods can variously produce sphere-like nanoparticles or nanoparticles with well-defined surface facets. The ability to control the crystal morphology and surface termination of faceted silicon nanoparticles is desirable from the point of view of creating nanoparticles with tunable optical properties for photovoltaics or optoelectronics, fine-tuned surface functionalization (e.g., for drug delivery), or with the ability to self-assemble into ordered structures. It is thus strongly desirable to understand how the detailed shape of silicon nanoparticles may be tuned by control of thermodynamic conditions (pressure, temperature, and chemical environment) during formation.

Silicon nanoparticles have been demonstrated in experiment using a broad variety of synthetic methods in the solid, liquid, gas, and plasma phases[5] and can be produced either in a solid matrix or as free-standing particles. Specific classes of techniques produce free-standing nanoparticles terminated with species such as hydrogen or halogen atoms. Because each adsorbed atom terminates a single silicon dangling bond and can adsorb only in a single configuration, these species allow flat surfaces with uniform termination to be readily formed. The formation of nanoparticles terminated with halogen species including chlorine, bromine, and iodine has been demonstrated[6−8] via gas- and liquid-phase methods. Halogen termination has also been used to enhance the efficiency of CdS quantum dot solar cells by passivating surface trap states following organic functionalization.[9] Compared to hydrogen termination, halogen termination offers several benefits, including the potential for a wider range of optimal nanoparticle shapes to be attained by the use of different halogens and the higher reactivity of halogen-terminated surfaces, which can make the subsequent functionalization of the nanoparticles with other (e.g., organic) groups easier.[6]

In recent work,[10] we studied the equilibrium surface termination and morphology of hydrogen-terminated silicon nanoparticles via ab initio thermodynamic calculations and demonstrated correspondence between our predicted nanoparticle shapes and those formed by gas-phase pyrolysis of silane.[11,12] Given the similar chemistry between hydrogen and the group VII elements fluorine, chlorine, bromine, and iodine, it is natural to ask how the surface energetics and nanoparticle shapes vary as the chemical identity of the adatom species progresses down group VII. In this work, we study the energetics of silicon surfaces terminated with F, Cl, Br, and I as a function of chemical potential, and we show how the optimal nanoparticle geometries and surface terminations vary due to the combination of chemical and steric effects presented by each element.

Received: April 22, 2014
Revised: June 20, 2014
Published: August 7, 2014

   dx.doi.org/10.1021/cg500558j | *Cryst. Growth Des.* 2014, 14, 4468−4474

CALCULATION METHODS

In this work, we use density functional theory to determine the surface energies of halogen-terminated silicon surfaces in the (100), (110), (111), and (113) planes. The computational methodology used is identical to that applied in Wilson and Barnard.[10] All surface energies in this work were computed using the VASP code[13] using pseudopotentials of the projector augmented wave type[14] and the exchange-correlation functional of Perdew, Burke, and Ernzerhof.[15] Kohn−Sham wave functions were represented in a plane wave basis set with a cutoff energy of 350 eV. The Brillouin zone was sampled with a k-point density that was equivalent to 12 × 12 for the Si(100) 1 × 1 structure, with the closest possible equivalent density used for other structures. Using these parameters, we found an equilibrium lattice constant for bulk silicon of 5.466 Å, which we use as the lattice constant for all slab calculations. The bulk lattice was found to have a ground-state internal energy of −5.424 eV/atom, which we use as the chemical potential for silicon.

All systems were simulated in slab geometries with the same termination on each surface. For Si(100), we used slabs of 18.08 Å thickness (thickness defined as the distance from the top to bottom atom in the bare configuration), for Si(110), slabs of 19.35 Å thickness, for Si(113), slabs of 24.82 Å thickness, and for Si(111), slabs of 19.53 Å for the (7 × 7) reconstruction (consisting of 596 silicon atoms in the bare configuration) and 24.08 Å in the (2 × 2) reconstruction. A vacuum spacing of at least 12 Å between the extremal silicon atoms of the slab and the slab's periodic image was used in each case.

SURFACE STRUCTURES

Four free-standing silicon surfaces have been observed to remain stable to further faceting: the (100), (110), (111), and (113) facets. Each facet may have multiple possible halogen terminations, depending on chemical potential. In this work, we computed the energetics of all known terminations of each surface that have been identified experimentally for hydrogen or halogens.

The bare Si(100) surface consists of of rows of silicon−silicon dimers, with two dangling bonds per dimer. At zero temperature, dimers buckle in alternate directions to form a $c(4 \times 2)$ structure. Termination of each dangling bond with an adatom leads to a 1 ML coverage.[16] If the surface dimer is broken and each end is terminated with another adatom, then this leads to a 2 ML coverage, which may be observed by adsorbing atomic hydrogen.[16] An intermediate 4/3 ML coverage is achievable, with alternate rows of dimers and undimerized double-terminated atoms. Finally, we have a 0.5 ML coverage, which may be achieved by terminating alternating dimers in a checkerboard pattern.

The as-cleaved Si(111) surface consists of an array of 3-fold-coordinated atoms. The ground state of the bare Si(111) surface is a complex 7 × 7 reconstruction,[17] known as the dimer-adatom-stacking fault (DAS) surface reconstruction.[18] For group VII adsorbates on Si(111), three different terminations have been observed. The first is a 7 × 7 19/49 monolayer structure that results from saturating the 19 surface dangling bonds of the DAS (7 × 7) reconstruction.[19] The second is the 7 × 1 structure with 43/49 monolayers, formed by the removal of the ad-dimers from the DAS surface and the saturation of the new dangling bonds thus created. Finally, we have the ideal 1 × 1 reconstruction in which every 3-fold-coordinated atom of the unreconstructed surface is terminated with a single adsorbate atom, which may be easily obtained experimentally for halogens.[20]

Cleavage of silicon along the (110) plane results in a (1 × 1) pattern in which each unit cell has two surface atoms, each 3-fold-coordinated, forming zigzag chains running in the $[1\bar{1}0]$ direction. Room-temperature reconstruction of the bare surface results in a complex (16 × 2) pattern, whose structure is yet fully understood;[21] however, termination of the surface leads to a simple 1 ML pattern in which each of the 3-fold-coordinated surface atoms acquires one adsorbate atom.[22] Because the structure of the (16 × 2) bare surface is not understood, we do not consider it in this work and consider only the (1 × 1) relaxed bare and 1 ML saturated surfaces. Because the reconstruction energy is likely to be small and the bare Si(110) surface is far from being the lowest-energy surface under any conditions, this approximation is justified.

The bare Si(113) surface reconstructs with a 3 × 2 symmetry,[23] which may be explained by the adatom-dimer-interstitial (ADI) model of Dąbrowski et al.[24] Experimental and computational studies have identified two possible saturation terminations for the Si(113) surface: one identified by Flege et al.[26] in chlorine and a second by Hara et al.[25] with hydrogen. The Flege et al. structure,[26] which they term a dimer-adatom-on-top (DAO) structure, consists of rows of silicon atoms terminated in three different ways: a silicon−silicon dimer, an adatom absorbed directly on top of a 3-fold-coordinated silicon, and a silicon adatom bonded to three first-layer silicons and terminated with an on-top terminating atom. The Hara structure is very similar, except that the dimer and on-top part of the motif are instead replaced with a silicon pentamer, which is itself terminated with an adatom.

RESULTS

Stable surface geometries were obtained using each halogen species for each possible termination, with the exception of the 2 ML Si(100) configuration, for which no stable geometry could be found with any species except hydrogen due to the extremely high adatom density. Calculated surface energies (in J m^{-2}) of all surface terminations are shown in Table 1, and surface stress (in J m^{-2}) for each surface configuration are shown in Table 2. Surface energies for hydrogen termination from Wilson and Barnard[10] obtained using the same methodology are also included for the purpose of comparison. These total energies are expressed relative to a reservoir of molecular halogen; that is, the difference in energy between two

Table 1. Surface Energy for Each Studied Surface Configuration[a]

	surface energy (J m^{-2})				
surface	H	F	Cl	Br	I
(100) bare	1.25	1.25	1.25	1.25	1.25
(100) 0.5 ML	0.75	−1.20	−0.08	0.12	0.38
(100) 1 ML	0.21	−3.67	−1.41	−0.99	−0.38
(100) 4/3 ML	0.16	−5.12	−1.67	−0.97	0.65
(111) bare (7 × 7)	1.22	1.22	1.22	1.22	1.22
(111) 19/49 ML	0.83	−1.00	0.03	0.20	0.41
(111) 43/49 ML	0.23	−3.70	−1.41	−0.98	−0.40
(111) 1 ML	0.07	−4.40	−1.77	−1.25	−0.46
(110) bare	1.49	1.49	1.49	1.49	1.49
(110) 1 ML	0.14	−5.12	−1.87	−1.11	0.56
(113) bare	1.28	1.28	1.28	1.28	1.28
(113) 1.5 ML (Flege[26])	0.35	−3.19	−1.13	−0.75	−0.22
(113) 1.5 ML (Hara[25])	0.39	−3.13	−1.10	−0.73	−0.24

[a]All total energies are relative to bulk silicon plus molecular X_2.

dx.doi.org/10.1021/cg500558j | Cryst. Growth Des. 2014, 14, 4468−4474

Table 2. Surface Stress for Each Studied Surface Configuration[a]

surface	stress (J m^{-2})				
	H	F	Cl	Br	I
(100) bare	−0.33	−0.33	−0.33	−0.33	−0.33
(100) 0.5 ML	−0.16	−0.48	−0.11	−0.10	−0.05
(100) 1 ML	−0.18	−0.81	−0.06	0.01	−0.21
(100) 4/3 ML	−0.20	−1.22	0.68	0.54	0.11
(111) bare (7 × 7)	−2.18	−2.18	−2.18	−2.18	−2.18
(111) 19/49 ML	−2.25	−3.41	−2.23	−2.23	−2.22
(111) 43/49 ML	−1.20	−3.63	−0.98	−0.86	−0.37
(111) 1 ML	−0.03	−0.83	0.10	0.15	0.43
(110) bare	−0.31	−0.31	−0.31	−0.31	−0.31
(110) 1 ML	−0.48	−1.12	−0.04	0.06	0.99
(113) bare	−0.59	−0.59	−0.59	−0.59	−0.59
(113) 1.5 ML	−0.58	−1.61	−0.69	−0.66	−0.56

[a]The 1.5 ML (113) termination refers to the Flege et al.[26] structure for H, F, Cl and Br and the Hara et al.[25] structure for I.

configurations with different coverage represents the energy needed to break apart the halogen dimer molecules to adsorb the halogen species on the surface.

Given these absolute surface energies, we may now compute the surface energy as a function of chemical potential μ. Under ordinary conditions, the gas- or liquid-phase chemical potential is negative, representing the free energy cost of removing a single molecule from its high-entropy fluid state to place it in a low-entropy state on the surface. We consider values of μ of between 0 and −5 eV per molecule, although we note that the low end of this scale may represent unrealistically low values of μ.

Figure 1 shows surface energy vs chemical potential for the (100) surface under each halogen species, with hydrogen also included for comparison purposes. For fluorine, the 4/3 ML Si(100) coverage, which has the highest adsorbate density of

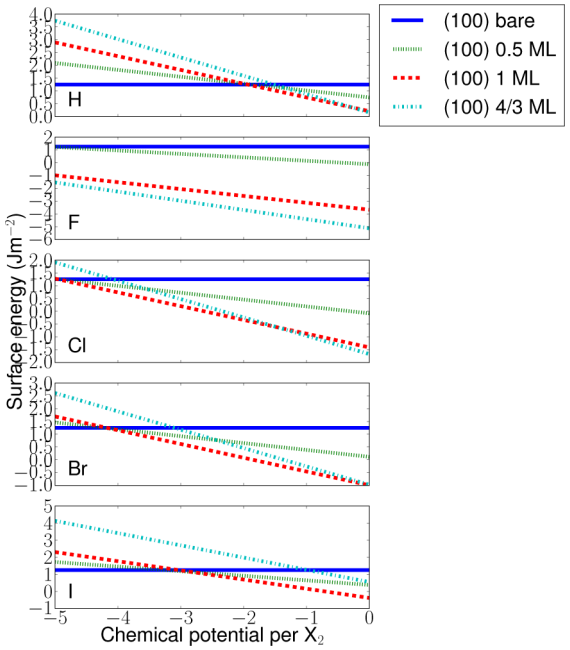

Figure 1. Relative surface energies of (100) surface reconstructions as a function of gas-phase chemical potential.

any achievable configuration, is the most stable surface reconstruction by a significant margin throughout the μ range of interest. For chlorine, much like hydrogen, the bare, 1 ML, and 4/3 ML surface terminations have regimes of stability, whereas the 0.5 ML termination remains unstable. For bromine, the 0.5 ML termination is stable in a small μ range, whereas the 4/3 ML termination is not stable for any negative value of μ. Iodine exhibits similar behavior to bromine, with all transitions shifted to higher μ.

For (111), we see a similar situation as that of (100) (Figure 2). Again, fluorine prefers full termination down to extremely

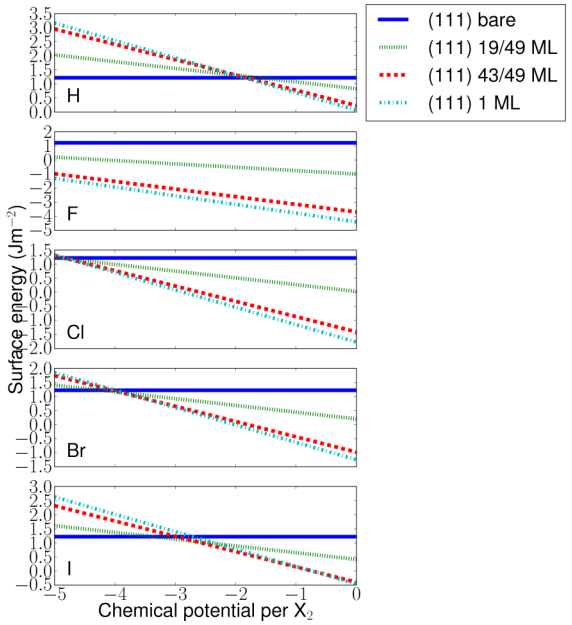

Figure 2. Relative surface energies of (111) surface reconstructions as a function of gas-phase chemical potential.

low values of the F_2 chemical potential. Hydrogen transitions directly from the bare (7 × 7) configuration to the fully terminated flat surface. For chlorine, however, an intermediate μ regime exists where the 19/49 ML partial termination becomes stable. Bromine has a regime of 19/49 ML stability, along with a regime where the 43/49 ML termination becomes stable. For iodine, these two regions of partial stability exist and are broader than those for bromine.

For the (110 surface), where only two surface phases are known, we find a transition from the bare to the fully terminated surface at −4.4, 3.4, and −1.3 eV for chlorine, bromine, and iodine, respectively (Figure 3). Because the bare (110) surface considered is the simple (1 × 1) surface rather than the (16 × 2) surface whose structure is unknown, the actual value of the transition μ may be slightly higher.

The situation for the (113) surface is similar to that for the (110) surface, with a transition from bare to full coverage occurring at progressively higher μ as the size of the halogen atom increases (Figure 4). Hydrogen, bucking the trend in this case, has a transition μ higher than iodine, reflecting the relative weakness of the Si−H bond compared to silicon−halogen bonds. In all cases, we find that the difference between the structures proposed by Flege et al.[26] and Hara et al.[25] is insignificant and that we cannot reasonably distinguish between the two, within the accuracy of this method.

dx.doi.org/10.1021/cg500558j | Cryst. Growth Des. 2014, 14, 4468−4474

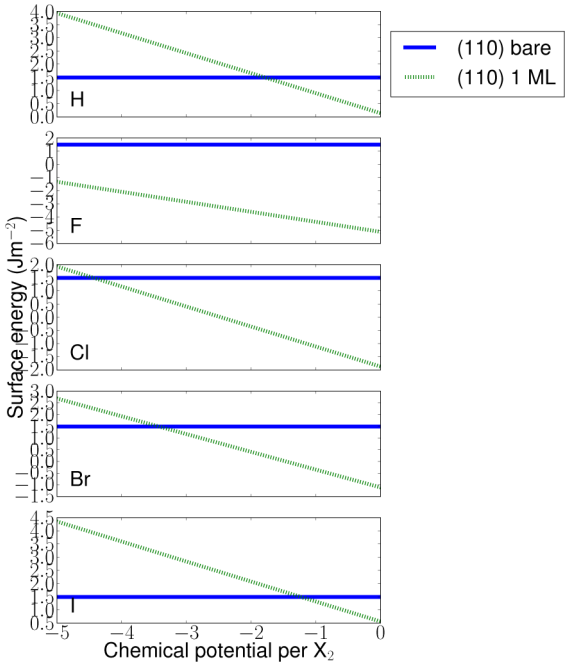

Figure 3. Relative surface energies of (110) surface reconstructions as a function of gas-phase chemical potential.

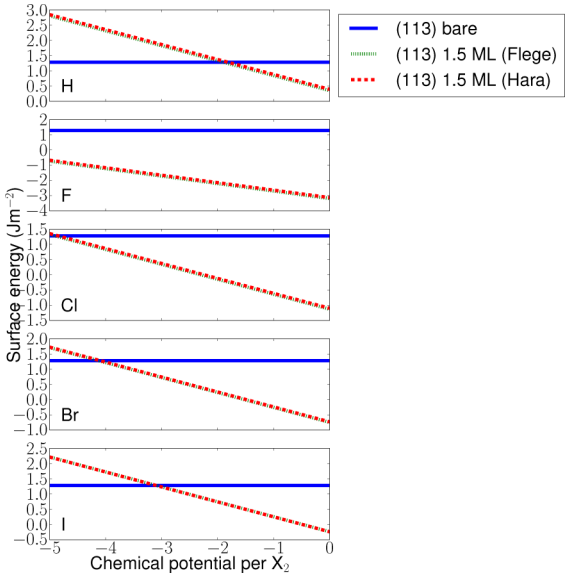

Figure 4. Relative surface energies of (113) surface reconstructions as a function of gas-phase chemical potential.

SURFACE PHASE DIAGRAM FOR ALL SURFACES

Given the absolute surface energies in Table 1, it is possible to compare the energetic stability of different surface orientations. In Figure 5, we plot an overall surface energy per unit area vs μ diagram for each halide species for all surface orientations. For simplicity and readability, only those surface orientations that are the ground state at some value of μ are shown. Results for hydrogen from Wilson and Barnard[10] are again included for the purposes of comparison.

For fluorine, the 4/3 ML Si(100) surface is the most stable by a significant margin throughout the μ range of interest, reflecting the extreme reactivity of Si with the F surface. Because of the substantial bonding energy associated with

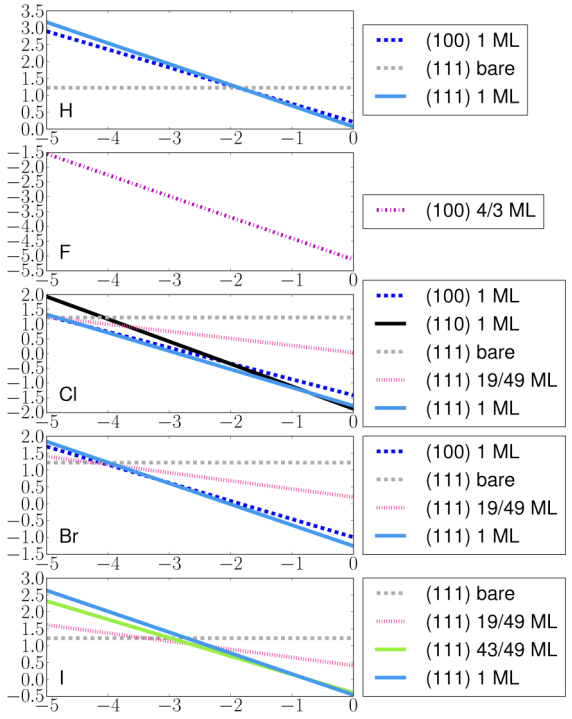

Figure 5. Surface energy vs μ for all surfaces and all halogen species, showing only the terminations that are optimal for some value of μ.

forming each Si–F bond, this surface, with the maximum density of adsorbate atoms for any surface, has by far the lowest surface energy. The surface energy is negative down to μ values of −7.2 eV, however, implying that solid fluorine-terminated silicon crystals cannot form for higher μ. This is consistent with fluorine's experimental tendency to etch silicon. Fluorine-terminated silicon surfaces are thus unlikely to be experimentally relevant, but the surface energies are included here for completeness and for an understanding of the relevant trends.

For chlorine, five different surfaces represent the ground state at some value of μ in the range of interest. The bare (111) surface is the ground state in the low μ limit, as is always the case. This transitions briefly into the 19/49 ML Si(111) in a small μ regime around −4.9 eV, then to the 1 ML Si(100), and then to the 1 ML Si(111). At μ values in excess of −0.8 eV, the saturated Si(110) surface is the ground state; however, the surface energy is negative for all values above μ = −2.8 eV.

For bromine, the situation is similar to that for chlorine, with the rapid succession of the bare (111), the 19/49 ML (111), the 1 ML (100), and the 1 ML (111) surfaces, all in a small μ range close to −4 eV. The surface energy becomes negative at μ = −2.2 eV.

For iodine, the situation is somewhat different. The Si(111) surface is the optimal configuration at all values of μ. In addition to the bare, 19/49, and 1 ML configurations, there is now a region of stability for the 43/49 ML configuration. Furthermore, the intermediate configurations now occupy a large portion of μ space from −3.4 to −1 eV. The surface energy becomes negative at −1 eV, implying that the fully saturated 1 ML configuration may never be the thermodynamic ground state for an iodine-terminated silicon surface.

dx.doi.org/10.1021/cg500558j | Cryst. Growth Des. 2014, 14, 4468–4474

OPTIMAL NANOPARTICLE SHAPES AND SURFACE TERMINATIONS

Having computed surface energy and stress as a function of chemical environment, we are in a position to predict nanoparticle shapes. In this work, we use a thermodynamic cartography model based on the surface energy and surface stress as used previously in several works.[10,27−30] The energetic cost of forming a nanoparticle of a particular size and shape is thus a sum of contributions from the formation of its surfaces, edges, and corners, with the latter two terms becoming less significant as the particle size is increased. Estimated silicon edge energies are on the order of 1.0×10^{-11} to 5.7×10^{-11} J m^{-2},[27] whereas surface energies are on the order of 1 J m^{-2}. Following Barnard and Zapol,[27] we estimate that the edge and corner energies are of limited significance for nanocrystals larger than 1.6 nm and can be safely neglected for nanoparticles larger than 7.3 nm. The effect of surface stress, which tends to compress the bulk-like portion of the nanoparticle resulting in an additional free energy term that depends on the bulk modulus B_0, is taken into account using a Laplace−Young formalism.[28] Further details on the present model may be found in Barnard.[29]

Figure 6 shows optimal silicon nanoparticle shapes for a fixed volume equivalent to that of a 10 nm diameter sphere. The dashed line separates nanoparticles whose overall surface energy is positive (on the left) from those whose surface energy is negative (on the right). Only a small variation in nanoparticle shape is seen with respect to size; particles at 4 nm are visually identical to those at 10 nm, and those at 1 nm diameter (beyond the regime of applicability of the model) show only modest variation (see the Supporting Information). All fluorine-terminated nanoparticles in the energy regime of interest will be energetically unstable, consistent with fluorine's strong tendency to etch silicon. For the remaining surface species, we see a progression of structures similar to that seen for hydrogen in Wilson and Barnard.[10] At low values of μ, nanoparticle shapes featuring the (111), (113), and (100) facets dominate. As chemical potential increases, we see a transition to truncated octahedral shapes consisting only of (100) and (111) facets, and then at relatively high μ, we find fully octahedral nanoparticle shapes.

Figures 7, 8, and 9 show in more detail the optimal morphologies for nanoparticles terminated by chlorine,

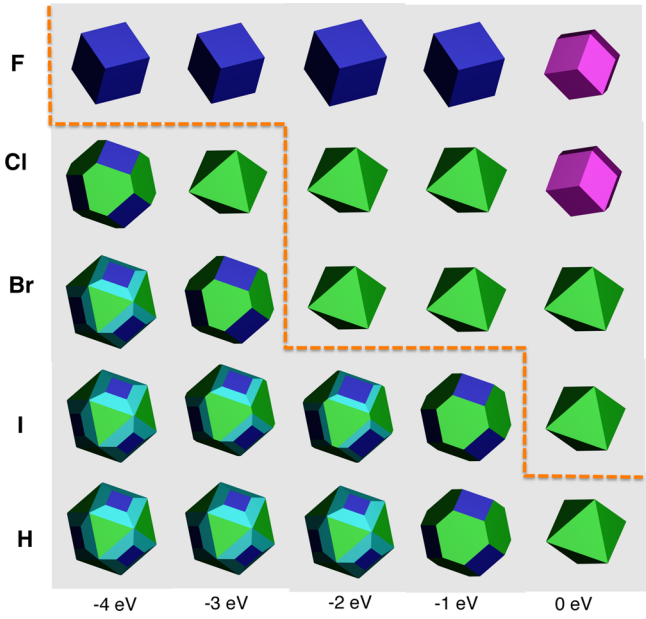

Figure 6. Optimal shapes of silicon nanoparticles as a function of chemical potential. The volume in each case is fixed as equivalent to a 10 nm silicon sphere. Nanoparticles to the right of the dashed line have a negative surface energy and hence are not stable in practice but are included for illustrative purposes. (111) facets are depicted in green, (113) facets, in cyan, (100) facets, in blue, and (110) facets (where present), in magenta.

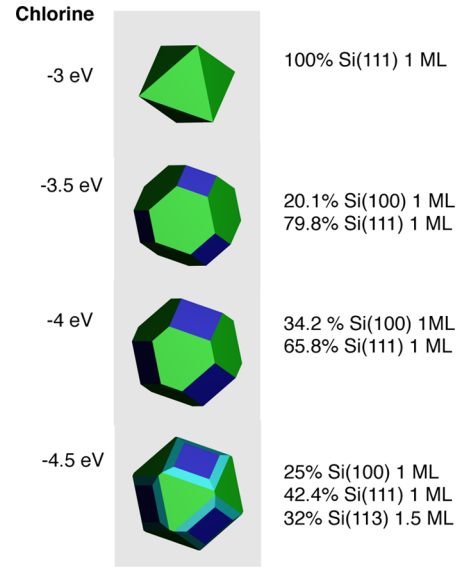

Figure 7. Optimal shapes and fractional surface terminations for chlorine-terminated silicon nanoparticles. The volume of each nanoparticle is equivalent to a 10 nm diameter sphere. (111) facets are depicted in green, (113) facets, in cyan, (100) facets, in blue, and (110) facets (where present), in magenta.

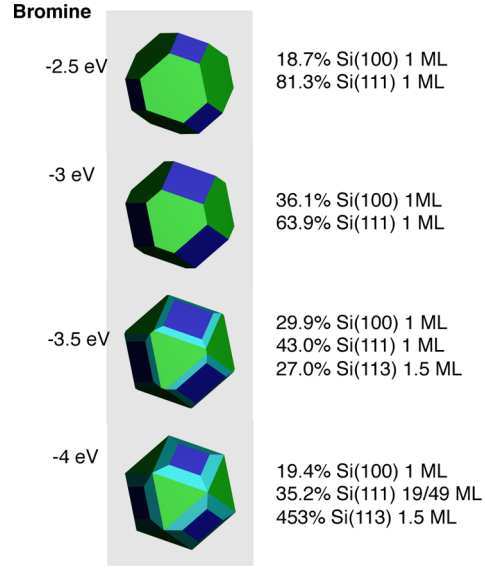

Figure 8. Optimal shapes and fractional surface terminations for bromine-terminated silicon nanoparticles. The volume of each nanoparticle is equivalent to a 10 nm diameter sphere. (111) facets are depicted in green, (113) facets, in cyan, (100) facets, in blue, and (110) facets (where present), in magenta.

dx.doi.org/10.1021/cg500558j | Cryst. Growth Des. 2014, 14, 4468−4474

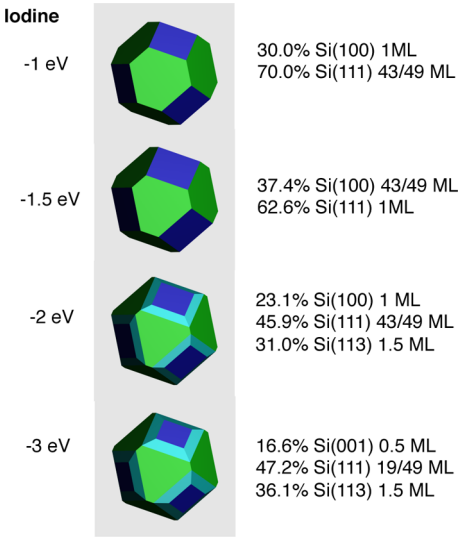

Figure 9. Optimal shapes and fractional surface terminations for iodine-terminated silicon nanoparticles. The volume of each nanoparticle is equivalent to a 10 nm diameter sphere. (111) facets are depicted in green, (113) facets, in cyan, (100) facets, in blue, and (110) facets (where present), in magenta.

bromine, and iodine in the regime where the surface energy remains positive, combined with the equilibrium chemical termination found on each surface. For chlorine, all surfaces remain fully terminated down to low values of μ. For bromine, we see a similar progression of structures, but the 19/49 ML termination is predicted on the Si(111) surfaces at μ below −3.5 eV. Notably, for iodine in a large μ regime from −3 to −1 eV, the equilibrium termination of the (111) facets is a partial termination (19/49 ML or 43/49 ML), whereas the (100) and (113) facets are maximally terminated. This suggests that equilibrium nanoparticles in this situation may be formed whose (111) facets may be more chemically reactive than that of the (100) and (113) facets, suggesting a possible route to selective functionalization of different nanoparticle facets.

DISCUSSION

Surface termination as a function of μ through the group of halogens and hydrogen provides an illustrative example of the competition between chemical bonding and steric effects in determining the thermodynamics of surface termination. Chemically, the energy gained by removing an atom from an X_2 dimer and bonding it with a surface silicon atom increases in the sequence H, I, Br, Cl, F, favoring the formation of increasingly high coverage surfaces. A second-order effect counteracting this is the steric hindrance between adjacent adatoms, which penalizes the denser packings as atom size increases. The relative stability of different surface orientations is governed by the interplay between these two effects.

Steric hindrance between adjacent adatoms, moreover, also leads to the stabilization of partial saturation coverages at intermediate μ values. For hydrogen and fluorine, the zero-temperature ground state of the Si(100) and Si(111) surfaces progresses directly from the bare to the fully saturated surface as μ is increased, implying that a state consisting of separate bare and fully terminated patches is preferable to the ordered intermediate coverage. For chlorine, bromine, and iodine, however, intermediate surface terminations including the 19/49 ML Si(111), the 43/49 ML Si(111), and the 0.5 ML Si(100), with an adsorbate to available site ratio of 39, 88, and 50%, respectively, attain regimes of stability. The ability to create nanoparticles with full termination on some surfaces but partial termination on others may have technological applications: If the partially terminated Si(111) surface of an iodine-terminated silicon nanoparticle can be induced to react with some functional group while the fully terminated Si(100) does not, then this may lead to the ability to create silicon nanoparticles with different terminations on each surface. For ligands other than halogens, many of which will be sterically larger than iodine, different saturation terminations may be available on each surface, and further work could determine optimal shapes for acquiring full or partial termination of these ligands. Understanding the dependence of the termination of each surface on chemical species and chemical potential may also assist in reducing defect concentrations. Future work may also explore whether different halogen terminations provide a better surface for the attachment of unreactive ligands.

In this work, we have focused solely on the evaluation of surface energies of surface reconstructions previously observed in experiment. The possibility that alternative surface terminations may exist at some value of μ should not be discounted, particularly for larger halogen atoms and for the Si(113) and Si(110) surfaces whose behavior has been less comprehensively studied in experiment. The effect of vibrational terms on the free energy has also been neglected; however, these should not form a dominant contribution. Moreover, finite temperature inevitably leads to the existence of defects, since configurational entropy ensures that for any finite temperature the thermodynamic ground state of a surface is not an ideal termination but a termination with some finite concentration of defects. This will have the effect of smoothing out the sharp transitions in our γ vs μ plots, but again, it should not fundamentally change the ordering of surfaces or substantially alter the overall predicted nanoparticle shapes.

CONCLUSIONS

We have presented surface energy calculations for halogen terminations of the silicon (100), (110), (111), and (113) surfaces as a function of gas-phase chemical potential and computed optimal shapes for halogen-terminated crystals using a nanomorphology model. For chlorine, bromine, and iodine, a variety of shapes including three, two, or one surface facet is achievable, while cube-like nanoparticles are the ground-state shape for fluorine at the extremely low μ values where nanoparticles are achievable. We have also shown that larger halides such as iodine form stable partial terminations at intermediate values of μ on the (100) and (111) surfaces, a fact that may potentially be exploitable for the purposes of selective functionalization of different surfaces. The results give a guide to the range of freestanding silicon nanoparticle shapes achievable in themodynamic equilibrium, and they demonstrate the possibility of utilizing steric effects to achieve nanoparticles that present multiple surface facets of differing reactivity. Future work to realize detailed thermodynamic control of nanoparticle shape experimentally or to establish the morphology of silicon nanoparticles terminated with other species theoretically may be valuable.

dx.doi.org/10.1021/cg500558j | Cryst. Growth Des. 2014, 14, 4468−4474

■ ASSOCIATED CONTENT

Supporting Information

Computed nanoparticle shapes as a function of size and chemical potential. This material is available free of charge via the Internet at http://pubs.acs.org.

■ AUTHOR INFORMATION

Corresponding Author

*E-mail: hughfw@gmail.com.

Notes

The authors declare no competing financial interest.

■ ACKNOWLEDGMENTS

This research was undertaken with the assistance of resources provided at the National Computational Infrastructure systems at the Australian National University under grant p00. The authors thank Cecilia Noguez for assistance with the Si(111) 7 × 7 geometry.

■ REFERENCES

(1) Boukamp, B. A.; Lesh, G. C.; Huggins, R. A. *J. Electrochem. Soc.* **1981**, *128*, 725−729.
(2) Liu, X. H.; Zhong, L.; Huang, S.; Mao, S. X.; Zhu, T.; Hyang, J. Y. *ACS Nano* **2012**, *6*, 1522−1531.
(3) Beard, M. C.; Knutsen, K.; Yu, P. R.; Luther, J.; Song, Q.; Metzger, W.; Ellingson, R. J.; Nozik, A. J. *Nano Lett.* **2007**, *7*, 2506−2512.
(4) Fujoka, K.; Hanada, S.; Kanaya, F.; Hoshino, A.; Sato, K.; Yokosuka, S.; Takigami, Y.; Hirakuri, K.; Shiohara, A.; Tilley, R. D.; Manabe, N.; Yamamoto, K.; Manome, Y. *J. Phys.: Conf. Ser.* **2011**, *304*, 012042.
(5) Mangolini, L. *J. Vac. Sci. Technol., B* **2013**, *31*, 020801.
(6) Shirahata, N.; Hozumi, A.; Yonezawa, T. *Chem. Rec.* **2005**, *5*, 145−149.
(7) Pettigrew, K. A.; Liu, Q.; Power, P. P.; Kauzlarich, S. M. *Chem. Mater.* **2003**, *15*, 4005−5011.
(8) Shirahata, N.; Furumi, S.; Sakka, Y. *J. Cryst. Growth* **2009**, *311*, 634−637.
(9) Ip, A. H.; et al. *Nat. Nanotechnol.* **2012**, *7*, 577−582.
(10) Wilson, H. F.; Barnard, A. S. *J. Phys. Chem. C* **2014**, *118*, 2580−2586.
(11) Körmer, R.; Butz, B.; Spiecker, E.; Peukert, W. *Cryst. Growth. Des.* **2012**, *12*, 1330−1336.
(12) Murthy, T. U. M. S.; Miyamoto, N.; Shimbo, M.; Nishizawa, J. *J. Cryst. Growth* **1976**, *33*, 1−7.
(13) Kresse, G.; Furthmüller, J. *Phys. Rev. B* **1996**, *54*, 11169−11186.
(14) Blochl, P. E. *Phys. Rev. B* **1994**, *50*, 17953−17979.
(15) Perdew, J. P.; Burke, K.; Ernzerhof, M. *Phys. Rev. Lett.* **1996**, *77*, 3865−3868.
(16) Boland, J. J. *Phys. Rev. Lett.* **1990**, *65*, 3325−3328.
(17) Takayanagi, K.; Tanishiro, Y.; Takahashi, S.; Takahashi, M. *Surf. Sci.* **1985**, *164*, 367−392.
(18) Brommer, K. D.; Needels, M.; Larson, B.; Joannopoulos, J. D. *Phys. Rev. Lett.* **1992**, *68*, 1355−1358.
(19) Noguez, C.; Beitia, C.; Preyss, W.; Shkrebtii, A. I.; Roy, M.; Borensztein, Y.; Sole, R. D. *Phys. Rev. Lett.* **1996**, *76*, 4923−4926.
(20) Eves, B. J.; Lopinski, G. P. *Surf. Sci.* **2005**, *579*, 89−102.
(21) Setvín, M.; Brázdová, V.; Bowler, D. R.; Tomatsu, K.; Nakatsuji, K.; Komori, F.; Miki, K. *Phys. Rev. B* **2011**, *84*, 115317.
(22) Arima, K.; Katoh, J.; Endo, K. *Appl. Phys. Lett.* **2004**, *85*, 6254−6256.
(23) Myler, U.; Jacobi, K. *Surf. Sci.* **1989**, *220*, 353−367.
(24) Dąbrowski, J.; Müssig, H.-J.; Wolff, G. *Phys. Rev. Lett.* **1994**, *73*, 1660−1663.
(25) Hara, S.; Suzuki, T.; Takahashi, I.; Ohsumi, T.; Fuse, K.; Fujishiro, H. I.; Irokawa, K.; Miki, H.; Kawazu, A. *e-J. Surf. Sci. Nanotechnol.* **2010**, *8*, 261−265.
(26) Flege, J. I.; Schmidt, T.; Siebert, M.; Materlik, G.; Falta, J. *Phys. Rev. B* **2008**, *78*, 085317.
(27) Barnard, A. S.; Zapol, P. *J. Chem. Phys.* **2004**, *121*, 4276−4283.
(28) Barnard, A. S. *J. Phys. Chem. B* **2006**, *110*, 24498−24504.
(29) Barnard, A. S. *Rep. Prog. Phys.* **2010**, *73*, 086502.
(30) Guo, H.; Barnard, A. S. *J. Mater. Chem.* **2011**, *21*, 11566−11577.